Apolipoprotein A-I Helix 6 Negatively Charged Residues Attenuate Lecithin−Cholesterol Acyltransferase (LCAT) Reactivity†

Eric T. Alexander,‡ Shaila Bhat,‡ Michael J. Thomas,§ Richard B. Weinberg,|| Victoria R. Cook,|| Manish S. Bharadwaj,‡ and Mary Sorci-Thomas*,‡,§

Departments of Pathology, Biochemistry, and Internal Medicine, Wake Forest University Health Sciences, Medical Center Boulevard, Winston-Salem, North Carolina 27157

Received December 9, 2004; Revised Manuscript Received January 31, 2005

ABSTRACT: Apolipoprotein A-I (apoA-I), the major protein in high density lipoprotein (HDL) regulates cholesterol homeostasis and is protective against atherosclerosis. An examination of the amino acid sequence of apoA-I among 21 species shows a high conservation of positively and negatively charged residues within helix 6, a domain responsible for regulating the rate of cholesterol esterification in plasma. These observations prompted an investigation to determine if charged residues in helix 6 maintain a structural conformation for protein−protein interaction with lecithin−cholesterol acyltransferase (LCAT) the enzyme for which apoA-I acts as a cofactor. Three apoA-I mutants were engineered; the first, $^3/_4$ no negative apoA-I, eliminated 3 of the 4 negatively charged residues in helix 6, no negative apoA-I (NN apoA-I) eliminated all four negative charges, while all negative (AN apoA-I) doubled the negative charge. Reconstituted phospholipid-containing HDL (rHDL) of two discrete sizes and compositions were prepared and tested. Results showed that LCAT activation was largely influenced by both rHDL particle size and the net negative charge on helix 6. The 80 Å diameter rHDL showed a 12-fold lower LCAT catalytic efficiency when compared to 96 Å diameter rHDL, apparently resulting from an increased protein−protein interaction, at the expense of lipid−protein association on the 80 Å rHDL. When mutant apoproteins were compared bound to the two different sized rHDL, a strong inverse correlation ($r = 0.85$) was found between LCAT catalytic efficiency and apoA-I helix 6 net negative charge. These results support the concept that highly conserved negatively charged residues in apoA-I helix 6 interact directly and attenuate LCAT activation, independent of the overall particle charge.

Numerous epidemiologic studies have demonstrated an association between plasma apoA-I[1] concentrations and a reduced risk for coronary heart disease in human populations (reviewed in *1*). Despite this strong association, little is known about how the structure of apoA-I contributes to its antiatherogenic properties. One hypothesis is that apoA-I HDL plays a central role in a process called reverse cholesterol transport (*2*−*4*). In this process, apoA-I first organizes and solubilizes phospholipid and cholesterol originating in the periphery, then it activates the enzyme LCAT converting cholesterol to cholesterol ester (CE), thereby promoting the maturation of nascent HDL particles from discs to spheres. The CE core of mature spherical HDL is subsequently removed by liver SR-B1 receptors (*5*) allowing cholesterol to be eliminated from the body via bile excretion. Another major role apoA-I plays in protecting against cardiovascular disease involves its role in modulating inflammation (*6*). While apoA-I structure clearly plays a major role in each of these mechanisms, the lack of a detailed lipid-bound apoA-I X-ray crystal structure hinders our understanding of its conformation at a protein−lipid interface (*7*).

In 1997, Borhani et al. published an X-ray crystal structure for lipid-free Δ43 apoA-I (*8*) which challenged the prevailing models describing the conformation of apoA-I. This study focused attention toward a new structure in which the apoprotein helices' lie perpendicular to the fatty acyl-chains of the bilayer resembling a "belt". Since then, a number of different studies covering a variety of approaches support this idea (*9*−*16*). Studies of other lipid-bound apolipoproteins, such as apoE (*17*) and apolipophorin III, a 17 kDa exchangeable insect apoprotein (*18*, *19*), provide additional support for a "belt" conformation.

Unique features of apoA-I include its 43 residue N-terminal globular domain, adjacent to a 200 residue region containing eight 22-amino acid repeating units and two 11-amino acid repeating units, all of which exhibit high α-helical, amphipathic character. Of these 10 helical segments, 7 are punctuated by proline residues and are important in providing stability for apoprotein−lipid interactions over

† These studies were supported by grants from the National Institutes of Health NHLBI HL-49373 and HL-64163 (M.S.T), HL-30897 (R.B.W.) and a Predoctoral Fellowship, NIH Training Grant HL-07115 (E.T.A).

* To whom correspondence should be addressed: Mary G. Sorci-Thomas, Ph.D., Professor of Pathology, Wake Forest University Health Sciences, Medical Center Blvd., Winston-Salem, NC 27157; phone, 336-716-2147; fax, 336-716-6279; e-mail, msthomas@wfubmc.edu.

‡ Department of Pathology.

§ Department of Biochemistry.

|| Department of Internal Medicine.

[1] Abbreviations: apoA-I, Apolipoprotein A-I; LCAT, lecithin−cholesterol acyltransferase; HDL, high-density lipoprotein; rHDL, reconstituted HDL; POPC, plamitoyl-oleoyl-phosphatidylcholine; POPS, palmitoyl-oleoyl-phosphoserine; $^3/_4$ NN apoA-I, $^3/_4$ no negative apoA-I; NN apoA-I, no negative apoA-I; AN apoA-I, all negative apoA-I; WT, wild-type.

10.1021/bi047412v CCC: $30.25
Published on Web 03/16/2005

the curved surface of a discoidal or spherical particle (*20*, *21*). Like all apoproteins in the supergene family, each of the repeating units in apoA-I are highly amphipathic exhibiting clear separation of their hydrophobic and hydrophilic faces when arranged on an Edmunson helical wheel. However, unlike the other related apoproteins, apoA-I contains almost exclusively class A_1 helices (*22*, *23*). The class A_1 helix is typified by the presence of two or more positively charged arginine residues flanking the interface between a highly conserved negatively charged face and the hydrophobic face of the amphiphathic helix. Although most of apoA-II's helices also contain positively charged residues at the hydrophilic−hydrophobic interface, these residues tend to be lysines rather than arginines and are thus designated class A_2 helices. The extent of charge conservation in both class A_1 and A_2 amphipathic helices is significant and has been hypothesized to play a role in stabilizing apoprotein helix−lipid interactions. In an attempt to explain the function of the highly conserved positively and negatively charged residues, one theory suggests that arginine residues orient toward the negatively charged phosphate groups associated with the phospholipid bilayer, stabilizing the apoprotein−lipid interactions (*22*). In other studies, a combination of experimental evidence and computer modeling suggests that positively charged arginines, specifically within helix 6, directly contribute to the activation of LCAT (*24*). Still other reports suggest that a balance between positively and negatively charged residues in apoA-I dictate the apoprotein's overall conformation and thus its ability to activate LCAT (*25*). In addition to these hypotheses, computer modeling studies of lipid-bound apoA-I (*21*, *26*) suggest that positively and negatively charged amino acid side chains participate in interhelical salt bridge formation conferring stability to apoA-I when bound to a phospholipid bilayer. In studies of other enzymes that catalyze reactions at a lipid interface, it has been shown that charged amino acids directly interact and promote catalysis through repulsive charge interactions (*27*, *28*). These studies show that the catalytic activity for a number of lipases and esterases correlate with a highly negative active site potential, suggesting that as the lipase releases free fatty acid from a triglyceride substrate the charged active site amino acids repel the newly formed fatty acid stimulating a another round of catalysis. Studies using both the cholesterol ester transfer protein and the phospholipid transfer protein show that a net negative charge strongly favors the optimal interaction at the apoprotein−lipid interface (*29*, *30*) thereby facilitating the overall reaction.

The studies described in this report were designed to probe the role of the highly conserved negatively charge residues found in apoA-I helix 6 and to elucidate their role in LCAT activation. Our results indicate that by increasing or decreasing the net negative helix 6 charge, the overall LCAT catalytic efficiency was significantly altered as a function of area constraints imposed on the rHDL particle. These results are highly suggestive of charged amino acids within apoA-I helix 6 attenuating the physiologically relevant activation domain of LCAT and thus the overall rate of cholesterol esterification.

EXPERIMENTAL PROCEDURES

Dithiothreitol, aprotinin, leupeptin, pepstatin, plamitoyl-oleoyl-phosphatidylcholine (POPC), and phenylmethylsulfonyl fluoride were purchased from Sigma. Palmitoyl-oleoyl-phosphoserine (POPS) was purchased from Avanti Polar Lipids. The mini-EDTA-free protease inhibitor tablets were purchased from Roche Molecular Biochem. Dithiobis-(succinimidylpropionate) (DSP) was purchased from Pierce. Oligonucleotides were synthesized by International DNA Technologies. Plasmid DNA was purified using the Wizard purification systems from Promega Inc. Deoxyribonuclease I (DNase I) was purchased from Worthington. The expression vector pTYB12, *Escherichia coli* strain ER2566, and chitin matrix were purchased from New England Biolabs. Restriction enzymes, T4 DNA ligase, DH5α competent cells, and isopropyl-*β*-D-thiogalactopyranoside were purchased from Invitrogen. Q-Sepharose Fast Flow matrix was purchased from Amersham Biosciences. Cholesterol (>99%) was from Nu-Chek Prep. Ultrafree-15 centrifugal units and Biomax 10K membranes were from Millipore Corporation. Sodium cholate was from Calbiochem, and all other chemical reagents were purchased from Sigma unless otherwise noted.

Mutagenesis of Human Apo A-I. The mutant $^3/_4$NN was constructed using the primer 5′GGCCAGCAGAGATGCGCAACCGCGCGCGCGCC3′ which changed the human WT apoA-I aspartic acids at positions 150 and 157 to asparagine and a glutamic acid at position 146 to a glutamine, where underlined bases denote the mutated codons; NN apoA-I was constructed using the polymerase chain reaction primer 5′ TGCGTGCGCAGCGCGTTCACATGGGCGCGCGCGCGGTTGCGCATCTGCTGGCCCAGTGGGCT 3′ which changed glutamic acids at positions 146 and 147 in the WT apoA-I to glutamines and aspartic acids at positions 150 and 157 to asparagines, and AN apoA-I was constructed using the primer 5′AGCTCGTCGCTGTAGGGGTCCAGATGGTCGCGCAGGTCGTCCACATGGTCGCGCGCGCG3′ which changed alanines at positions 154, 158, and 164 and the threonine at position 161 to aspartic acids. The 5′ and 3′ end-most primers used to complete the mutant apoA-I cDNA were the same as described previously (*31*), and the cDNA was cloned into the pTYB12 vector.

Expression and Purification of Wild-Type and Mutant ApoA-I. ER2566 *E. coli* cells were transformed with the appropriate mutant apoA-I cDNA, induced with isopropyl-*β*-D-thiogalactopyranoside grown at 16 °C overnight. The expressed protein was purified from cell extracts as previously described (*31*). After the final purification, lyophilized mutant apoA-I was taken up in 6 M guanidine hydrochloride and dialyzed against 10 mM ammonium bicarbonate, pH 7.4, containing 3 *μ*M EDTA and 15 *μ*M sodium azide. The protein purity and molecular weight were determined using a Quattro II mass spectrometer as previously reported (*31*, *32*).

Preparation of 96 Å and 80 Å rHDL Particles. The recombinant HDL containing $^3/_4$ NN, NN, and AN apoA-I were prepared using the sodium cholate dialysis method (*33*, *34*). The rHDL with an approximate diameter of 96 Å were prepared with POPC at a starting molar concentration of 80 POPC/5 cholesterol/1 apoA-I. After extensive dialysis to remove the sodium cholate, the rHDL were purified by FPLC using three Superdex 200 HR 10/30 columns linked in tandem and run at a flow rate of 0.5 mL/min in 0.9% NaCl, 1.5 mM sodium azide, and 0.3 mM EDTA at pH 7.4. Pooled fractions corresponding to the eluted rHDL were concentrated using Amicon Ultra-15 10 000 MWCO centrifugal filter

devices and then assayed for phospholipids, cholesterol, and protein content as described (*31*−*33*). The rHDL containing the negatively charged phospholipid, POPS, were prepared in a manner similar to that described above except that the starting molar ratio was 76 mol POPC/4 mol POPS and 5 mol cholesterol/1 mol apoA-I. Final molar content of POPS in the rHDL was assayed as described previously (*35*).

POPC-containing rHDL with an approximate diameter of 80 Å were prepared using the sodium cholate methods, except that the starting molar ratio was 24 mol POPC/5 mol cholesterol/1 mol apoA-I. The purification of small rHDL required ultracentrifugation at 50 000 rpm for 18 h in a Ti-70.1 rotor prior to FPLC purification to remove excess apoA-I. Cross-linking was carried out as previously described (*16*) on all rHDL preparations to determine the number of apoA-I molecules per particle.

Particle Homogeneity Using 4−*30% Nondenaturing Gradient Gel Electrophoresis.* The diameter of 96 and 80 Å POPC rHDL were determined using 4−30% nondenaturing gradient gel electrophoresis as previously described (*16*, *32*). Gels were run at 2800 V/hr to ensure that the particles had migrated to equilibrium then fixed and stained as described previously. The rHDL particle size was determined by comparison to protein standards of known Stokes' diameter as described (*32*, *36*).

Surface Charge Determination Using 0.5% Agarose Gel Electrophoresis. The rHDL surface charge was measured by determining the relative electrophoretic mobility of wild-type and mutant apoA-I containing rHDL by separation on a 0.5% agarose gel (Beckman Coulter, Paragon) as described (*37*). Briefly, 5 μg of rHDL protein was loaded per lane and run for approximately 2.5 h at 100 V according to manufactures instructions. The gels were fixed for 5 min, dried for 1 h at 80 °C, then stained with Paragon Lipostain. Surface charge for each rHDL was calculated as described previously (*37*).

LCAT Reaction Kinetics. The LCAT reaction was monitored by following the conversion of radiolabeled cholesterol to radiolabeled cholesterol ester using POPC rHDL containing either WT or mutant apoA-I or using POPC/POPS rHDL containing WT apoA-I as previously described (*31*, *33*). The complexes were assayed in triplicate using 0−3.0 μg of substrate cholesterol in a final concentration of 10 mM Tris, pH 7.4, 140 mM NaCl, 0.25 mM EDTA, 0.15 mM sodium azide, 0.6% fatty acid-free bovine serum albumin, 2 mM β-mercaptoethanol, and 20−80 ng of recombinant His-tag LCAT (*38*). The reactions were carried out for 10−120 min at 37 °C, and the conversion of [^{3}H]cholesterol to [^{3}H]-cholesterol ester was determined after lipid extraction of the incubation mixture followed by thin-layer chromatography. The extent of cholesterol esterification was kept below 15% to maintain first-order kinetics. The fractional cholesterol esterification rate was expressed as nanomoles of cholesterol ester formed per hour per milliliter of LCAT. Apparent V_{max} and K_m values were determined from Hanes−Woolf plots (*31*, *33*) of rHDL cholesterol substrate concentration divided by the cholesterol ester formation rate versus HDL cholesterol substrate concentration.

Circular Dichroism Spectroscopy. Circular dichroism spectra were recorded with a Jasco J720 spectropolarimeter at 25 °C using a 0.1 cm path length cell. Ellipticity was measured at 222 nm. Five scans were recorded and averaged, and the background was subtracted. Mean molar residue ellipticity (q) is reported as degrees cm^2 dmol^{-1} and calculated from the equation, $[q] = (q_{obs}115)/(10lc)$, where q_{obs} is the observed ellipticity at 222 nm in degrees, 115 is the mean residue molecular weight of the protein, l is the optical path length in centimeters, and c is the protein concentration in g/mL. The percent α-helix content was calculated from the formula $[q]_{222} = (-30\,300f_h) - 2340$ as previously described (*33*).

Interfacial Exclusion Pressure at Air/Water Interface. The interfacial exclusion pressure of recombinant apolipoproteins at the phospholipid/water interface was determined using a KSV 5000 Langmuir film balance (KSV Instruments, Helsinki, Finland) as previously described (*39*, *40*). Dioleoylphosphocholine monolayers were spread at the air/buffer interface at initial pressures of 5−30 mN/m, and then WT or mutant apoA-I was injected into the subphase to give a final concentration of 50 μg/dL, which had been previously determined to yield saturating binding to the interface. The increase in interfacial pressure was then monitored by a Wilhelmy plate until it reached a stable plateau. The interfacial exclusion pressure was determined by extrapolation of the change in pressure versus the initial pressure.

Data Analysis. Data are presented as the mean ± SD. Data were analyzed using Student's t test with the Statview 5.0.1 program, and then individual differences between pairing of groups were found using Fisher's least significant posthoc test.

RESULTS

Positional Conservation of Negative and Positive Charge within ApoA-I Helix 6. ApoA-I helices 6 and 7 have been shown to be essential for LCAT (*7*, *41*−*44*) activation and belong to a group of amphipathic α-helices designated as class A_1. This distinct class of amphipathic α-helix is found exclusively in apoA-I (*22*, *23*) and is distinguished from other classes of amphipathic helices by possessing clearly delineated negative and positively charged residues when arranged on a Edmunson helical wheel, as shown in Figure 1, panel A. For comparison, a diagram of the eight remaining apoA-I helices was also constructed, as shown in Figure 1, panel B. Examination of these two diagrams shows that while helices 6 and 7 show a high degree of positional side chain conservation with respect to both negatively and positively charged residues, the other eight helices in apoA-I are not as highly conserved at these same positions (*24*). Instead, apoA-I helices 1−5 and 8−10 appear to have positively and negatively charged residues interspersed randomly within the hydrophilic face of the helix with the exception of a single position, as indicated by a black arrow (Figure 1, panel B). These comparisons suggest that the positional side chain conservation of positively and negatively charged residues within helices 6 and 7 is greater than the conservation of negatively charged residues observed in the other eight helices within apoA-I.

On the basis of the above comparison of charged residue placement and conservation, we constructed a series of apoA-I mutants that differed in their overall helix 6 net negative charge, based on the human wild-type (WT) helix 6 sequence, shown in Figure 1C. The first mutant, termed E146Q, D150N, D157N apoA-I or "$^3/_4$ no negative apoA-I"

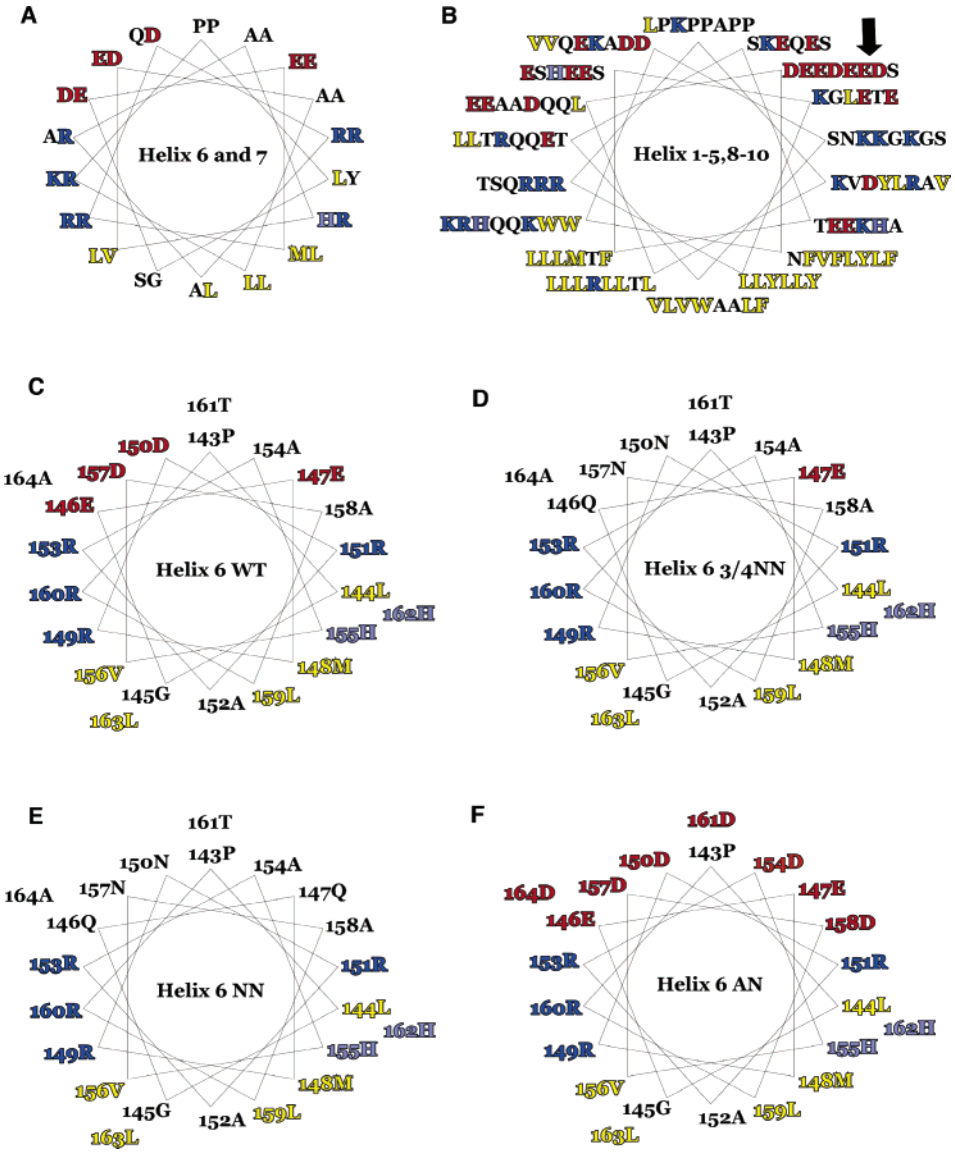

FIGURE 1: Edmunson helical wheel alignments of apoA-I helix units 1−10. (A) Shows the alignment and charge distribution comparing helices 6 and 7 of apoA-I; (B) shows the comparison of all remaining helices 1−5 and 8−10, arranged on an Edmunson helical wheel, where residues are separated by approximately 100°, with the lowest numbered residues starting on the inside progressing to the highest numbered on the outside of the helix; (C) shows the helical wheel alignment for wild-type apoA-I helix 6; (D) shows the alignment for $^3/_4$ no negative apoA-I ($^3/_4$ NN apoA-I = E146Q, D150N, D157N apoA-I); (E) shows no negative apoA-I helix 6 (NN apo A-I = E146Q, E147Q, D150N, D157N apoA-I), and (F) shows all negative apoA-I helix 6 (AN apoA-I = A154D, A158D, T161D, A164D apoA-I). Hydrophobic residues are colored yellow, positively charged residues are colored blue, and negatively charged residues are in red. The high conservation of charged residues within helices 6 and 7 was not generally observed in the remaining apoA-I helices, except in a position (black arrow) where negatively charged residues were found (panel B).

($^3/_4$ NN apoA-I), removes three of the four naturally occurring negatively charged residues in helix 6, as shown in Figure 1D. The second mutant, E146Q, E147Q, D150N, D157N apoA-I or "no negative apoA-I" (NN apoA-I), removes all four negatively charged residues in helix 6, thus giving an overall net positive charge to the helix, shown in Figure 1E. The third mutant, A154D, A158D, T161D, A164D or "all negative apoA-I" or (AN apoA-I), places four new negatively charged residues in addition to the four naturally occurring negative charges bringing the total to eight negatively charged residues within helix 6, shown in Figure 1F.

Changes in ApoA-I Helix 6 Negative Charge Alters Particle Diameter and α*-Helical Content.* To test the ability of these proteins to bind and organize phospholipids, POPC rHDL containing apoA-I were prepared with a starting molar phospholipid/cholesterol/apoA-I ratio of 80:5:1 and yielded particles of approximately 96 Å in diameter, while particles prepared at a starting molar ratio of 24:5:1 yielded discs of about 78−80 Å in diameter, as shown in Figure 2, panels A and B. Final molar compositions were performed on purified POPC rHDL particles of both molecular diameters and are listed in Table 1. These data show that both $^3/_4$ NN and NN apoA-I but not the AN rHDL contained 20% more POPC per particle, regardless of particle diameter, than WT apoA-I rHDL. An increase in phospholipid content is consistent with the 2−4 Å increase in molecular diameter of $^3/_4$ NN and NN apoA-I rHDL (Table 1). This modest but highly reproducible size difference in $^3/_4$ NN and NN apoA-I rHDL particle diameter was confirmed when rHDL particles were analyzed by two-dimensional nondenaturing gel electrophoresis methods (B. Asztalos, unpublished observations) (*45*, *46*).

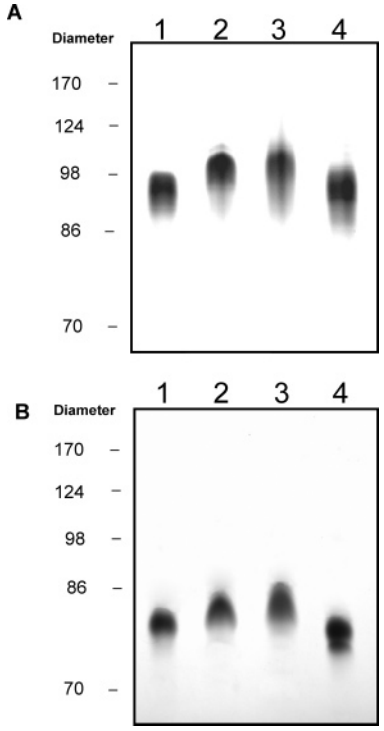

FIGURE 2: Coomassie blue stained 4−30% nondenaturing polyacrylamide gradient gel of POPC rHDL. (A) The 96 Å POPC rHDL were prepared at a starting molar ratio of 80:5:1, phospholipid/cholesterol/apoA-I, and (B) the 80 Å POPC rHDL were prepared at a starting molar ratio of 24:5:1, phospholipid/cholesterol/apoA-I. (A and B) Lane 1, WT apoA-I rHDL; lane 2, $^3/_4$ NN apoA-I rHDL; lane 3, NN apoA-I rHDL; and lane 4, AN apoA-I rHDL. All 96 Å POPC rHDL were purified by FPLC, while all 80 Å rHDL were purified by a combination of ultracentrifugation and FPLC as described in Experimental Procedures. Calibrating high-molecular weight standards corresponded to a Stokes' diameter: thyroglobin, 170 Å; ferritin, 124 Å; catalase, 98 Å; lactate dehydrogenase, 86 Å; serum albumin, 74 Å.

Next, the α-helical content of each mutant rHDL was evaluated to determine whether the addition or deletion of negative changes altered apoprotein secondary structure as shown in Table 2. Generally, any of the alterations in apoA-I helix 6 charge resulted in a ∼40% reduction in α-helical content for the lipid-free proteins (data not shown). However, in the lipid-bound state, the 96 Å $^3/_4$ NN apoA-I and NN apoA-I but not the 80 Å counterpart demonstrated a significant increase in α-helical content suggesting that these mutant proteins increased their interaction with phospholipids, consistent with the larger rHDL diameter and lipid content of the particles containing these mutant proteins (Tables 1 and 2).

Overall, the increase in AN apoA-I rHDL helix 6 negative charge was associated with a decrease in α-helical content (Table 2). While the 96 Å AN apoA-I rHDL only showed a trend toward such a decrease, the 80 Å AN apoA-I rHDL had a statistically significant reduction in α-helical content, consistent with the loss of lipid−protein interactions. It has been shown that an increase in α-helicity is a major driving force in stabilizing apoA-I phospholipid interactions (*47*). It is believed that the N-terminal half of apoA-I is responsible for most of the α-helical structure and the marginal stability of lipid-free apoA-I, while the C-terminus (no. 190−243) is responsible for the large increase in α-helical content when apoA-I binds to lipid (*48*). Investigations of the central region

Table 1: Recombinant HDL Composition and Particle Size[a]

recombinant HDL discoidal complexes[b]	final POPC/apo A-I molar ratio	final cholesterol/apo A-I molar ratio	particle diameter Å
	96 Å rHDL[c]		
WT apoA-I	71 ± 7[e]	5.7 ± 1.0[e]	96 ± 3[e]
$^3/_4$ NN apoA-I	87 ± 6[f]	4.9 ± 1.3[e,f]	98 ± 5[f]
NN apoA-I	92 ± 8[f]	4.8 ± 0.7[e,f]	100 ± 2[f]
AN apoA-I	68 ± 3[e]	4.0 ± 0.6[f]	94 ± 1[e]
	80 Å rHDL[d]		
WT apoA-I	34 ± 3[g]	6.7 ± 1.2[g]	81 ± 2[g]
$^3/_4$ NN apoA-I	40 ± 2[h]	8.7 ± 2.9[g]	84 ± 3[g]
NN apoA-I	37 ± 2[h]	5.9 ± 1.4[g]	85 ± 3[g]
AN apoA-I	34 ± 4[g]	5.8 ± 1.8[g]	79 ± 2[g]

[a] Final molar ratios on all rHDL were determined after purification as described under Experimental Procedures with each molar composition and particle diameter representing the average of 2−5 individual rHDL preparations. The rHDL diameters were determined by 4−30% nondenaturing gradient gel electrophoresis. All preparations of rHDL contained two molecules of apoprotein per particle, as determined by cross-linking with dithiobis(succinimidylpropionate) as described under Experimental Procedures. [b] Wild-type apoA-I = WT apoA-I; $^3/_4$ NN or $^3/_4$ no negative apoA-I = E146Q, D150N, D157N apoA-I; NN apo A-I or no negative apoA-I = E146Q, E147Q, D150N, D157N apoA-I; AN apoA-I or all negative apoA-I = A154D, A158D, T161D, A164D apoA-I. [c] The starting molar ratio for 96 Å rHDL was 80:5:1 plamitoyl-oleoyl-phosphatidylcholine (POPC)/cholesterol/apoA-I. [d] The starting molar ratio for 80 Å rHDL was 24:5:1 POPC/cholesterol/apoA-I. [e−h] All values represent the mean ± SD. Values marked with different letters were found to be statistically different at $p < 0.05$.

(no. 144−165) show that helix 6 is essential for the overall protein conformation, stability, phospholipid binding (*49*), and the disordered state of region no. 123−142. Thus, it is possible that the removal of helix 6 negative charge on 96 Å rHDL allows greater interaction with the lipid, while in the restricted environment of the 80 Å rHDL, removal of the negative charge has no effect on secondary structure. Conversely, the addition of helix 6 negative charge causes a reduction in lipid−protein interaction on 96 Å rHDL, with the reduction in α-helicity becoming accentuated when AN apoA-I is confined to the restricted environment of the smaller (80 Å) diameter rHDL.

Particle Diameter and Net Negative Charge Attenuate LCAT Reactivity. Next, LCAT activation properties were measured for mutant and WT apoA-I rHDL after particle diameters and composition were measured. Table 2 shows that the apparent K_m was relatively unchanged for both the 96 and 80 Å particles. However, a large and highly significant 13-fold reduction in the K_m was seen for 80 Å WT apoA-I rHDL when compared to 96 Å WT apoA-I rHDL. This trend was also seen for each of the 80 Å mutant apo A-I rHDL when compared to their 96 Å rHDL equivalent. Because the K_m is believed to be a measure of the enzyme's overall binding affinity to the rHDL substrate, this decrease in the K_m has been attributed to changes in lipid packing on the disc which occur as the apoprotein adapts to the smaller diameter of the particle (*14*, *50*−*52*). Thus, the K_m appeared to be greatly affected by the change in particle diameter but not greatly affected by the alteration in helix 6 charge.

Unlike the trend seen for the K_m, the V_{max} or maximum reaction velocity was not significantly different between 96 and 80 Å WT apoA-I rHDL (*50*). In fact, the V_{max} was only significantly reduced by alteration in the net helix 6 charge.

Table 2: Reaction Kinetics of Recombinant HDL Particles with LCAT[a]

recombinant HDL substrate[b]	α-helicity[c] (%)	apparent K_m (μM)	apparent V_{max} (nmol/(h mL))	apparent V_{max}/K_m (nmol/(h mL μM))	net negative charge of 2 Apo-Is per rHDL[d]
			96 Å rHDL[e]		
WT apoA-I	72 ± 5[f]	1.0 ± 0.2[f]	3016 ± 195[f]	3341 ± 489[f]	−20
3/4 NN apoA-I	93 ± 5[g]	0.6 ± 0.1[f]	1246 ± 57[g]	1986 ± 183[g]	−14
NN apoA-I	93 ± 8[g]	1.4 ± 0.8[f]	1477 ± 210[g]	1372 ± 475[g]	−12
AN apoA-I	70 ± 3[f]	0.5 ± 0.3[g]	1374 ± 344[g]	3199 ± 977[f]	−28
			80 Å rHDL[e]		
WT apoA-I	65 ± 3[h]	13.0 ± 7.9[h]	3222 ±301[h]	288 ± 169[h]	−20
3/4 NN apoA-I	65 ± 2[h]	12.1 ±11.3[h]	1670 ± 14[i]	137 ± 19[i]	−14
NN apoA-I	64 ± 16[h,j]	16.8 ± 7.5[h]	1883 ± 77[i]	123 ± 50[i]	−12
AN apoA-I	59 ± 5[i,j]	9.3 ± 7.3[h]	549 ± 281[j]	78 ± 46[i]	−28

[a] Apparent kinetic parameters were determined from Hanes−Woolf plots of reaction velocity and cholesterol concentration as described in Experimental Procedures. All values represent the mean ± SD of triplicate determinations on three or more independent rHDL preparations. All preparations of rHDL contained two molecules of apoA-I per particle. [b] WT apoA-I = Wild-type apoA-I; 3/4 NN or 3/4 no negative apoA-I = E146Q, D150N, D157N apoA-I; NN apo A-I or no negative apoA-I = E146Q, E147Q, D150N, D157N apoA-I; AN apoA-I or all negative apoA-I = A154D, A158D, T161D, A164D apoA-I. [c] α-helicity was determined using a Jasco J720 spectropolarimeter to measure the ellipticity at 222 nm. [d] Calculated from the net charge of 243 amino acids in full length apoA-I at pH 7.4. [e] The 96 Å and 80 Å rHDL were prepared as described in Table 1. [f−j] Values marked with different letters were found to be statistically different at $p < 0.05$.

Table 2 shows that all but one mutant apoA-I rHDL showed a 2-fold reduction in V_{max} independent of whether the particles were 96 or 80 Å. The exception, 80 Å AN apoA-I rHDL, showed a 6-fold lower V_{max} when compared to 80 Å WT apoA-I rHDL. This dramatic reduction in the AN apoA-I rHDL reaction rate was seen only in the 80 Å rHDL, readily apparent from the kinetic curves, as shown in Figure 3.

A combined mathematical representation of both the V_{max} and K_m conveys a relationship termed catalytic efficiency (V_{max}/K_m), which represents the overall capacity of LCAT to generate cholesterol esters. In 96 Å rHDL, the catalytic efficiency was significantly reduced by a decrease in helix 6 negative charge and unchanged by the increase in helix 6 negative charge. A similar trend was also seen in the 80 Å rHDL, which showed a 2-fold reduction in catalytic efficiency when the helix 6 negative charge was decreased. The exception to this trend was the 80 Å AN apoA-I rHDL, which showed a 4-fold lower catalytic efficiency compared to 80 Å WT apoA-I rHDL (Table 2). This large decrease in LCAT catalytic efficiency appears to have resulted entirely from a reduction in V_{max} presumably due to the increase in helix 6 negative charge.

To probe this relationship further, the LCAT catalytic efficiency (Table 2) was plotted against the net negative charge for each of the 96 Å rHDL studied (Table 2) and is shown in Figure 4, Panel A. These data show that a significant inverse correlation ($r = -0.85$) for the 96 Å rHDL exists, suggesting that the net helix 6 charge modulates LCAT catalyzed cholesterol esterification. Figure 4B shows that a similar inverse relationship was also seen for 80 Å rHDL, with the exception of AN apoA-I rHDL. The apparent disconnection between AN apoA-I rHDL's catalytic efficiency and the correlation with increased negative charge suggests that the interaction between apoA-I helix 6 and LCAT is adversely affected by the combination of increased helix 6 negative charge and the altered conformation of the mutant protein on the smaller rHDL particles. These results strongly suggest that LCAT directly interacts with helix 6 and that, by increasing the negative charge, the optimal enzyme−protein interaction for activation is dramatically reduced. Another possibility exists, however, that instead of helix 6 directly interacting with LCAT, the charge-induced conformational changes on an 80 Å rHDL does not allow proper "presentation" of the phospholipids' substrate to the enzyme, thus reducing the catalytic activity.

Helix 6 Negative Charge and Surface Activity. To address whether apoA-I helix 6 net charge alters the lipid-binding properties of apoA-I, we investigated the surface activity of each of the mutant proteins by measuring their exclusion pressure at a phospholipid/water interface, also referred to as the surface activity. Studies have shown that interactions of apoA-I with a hydrophobic surface are mediated by its amphipathic α-helices such that the interaction energy of a given helix with the lipid interface is a function of its amphipathicity (*53*). The mean hydrophobic moment which quantifies the amphipathicity of a given helical region can approximate the surface activity of an apoprotein (*54*, *55*). Table 3 lists the calculated hydrophobicity and hydrophobic moment of helix 6 in WT and each of the mutant apoA-I's and the exclusion pressure of each parent protein. The results show that the surface activity for AN apoA-I was significantly lower (30%) when compared to WT apoA-I presumably due to changes in hydrophobicity and hydrophobic moment of helix 6 (Table 3). These results suggest that by increasing the net helix 6 negative charge, AN apoA-I is less able to penetrate the lipid monolayer and form stabilizing α-helical structures with the lipid interface. These findings are consistent with the finding that AN apoA-I has less α-helical content on the 80 Å discs since it appears to have a compromised ability to engage in lipid−protein interactions when confined to the area of an 80 Å rHDL.

Does Negative Particle Charge or Negative Apoprotein Charge Alter LCAT Catalytic Activity? The LCAT kinetic studies shown here indirectly suggest that helix 6 negative charge interacts directly with the enzyme; however, it is also possible that negatively charged residues in helix 6 may cause interfacial lipid effects as the enzyme binds to the rHDL particle. Therefore, to distinguish between these possibilities, the rHDL phospholipids were enriched in negatively charged species, and the LCAT activation properties were assessed. The rHDL were generated containing the negatively charged phosphoserine (POPS) at molar ratios mimicking the in-

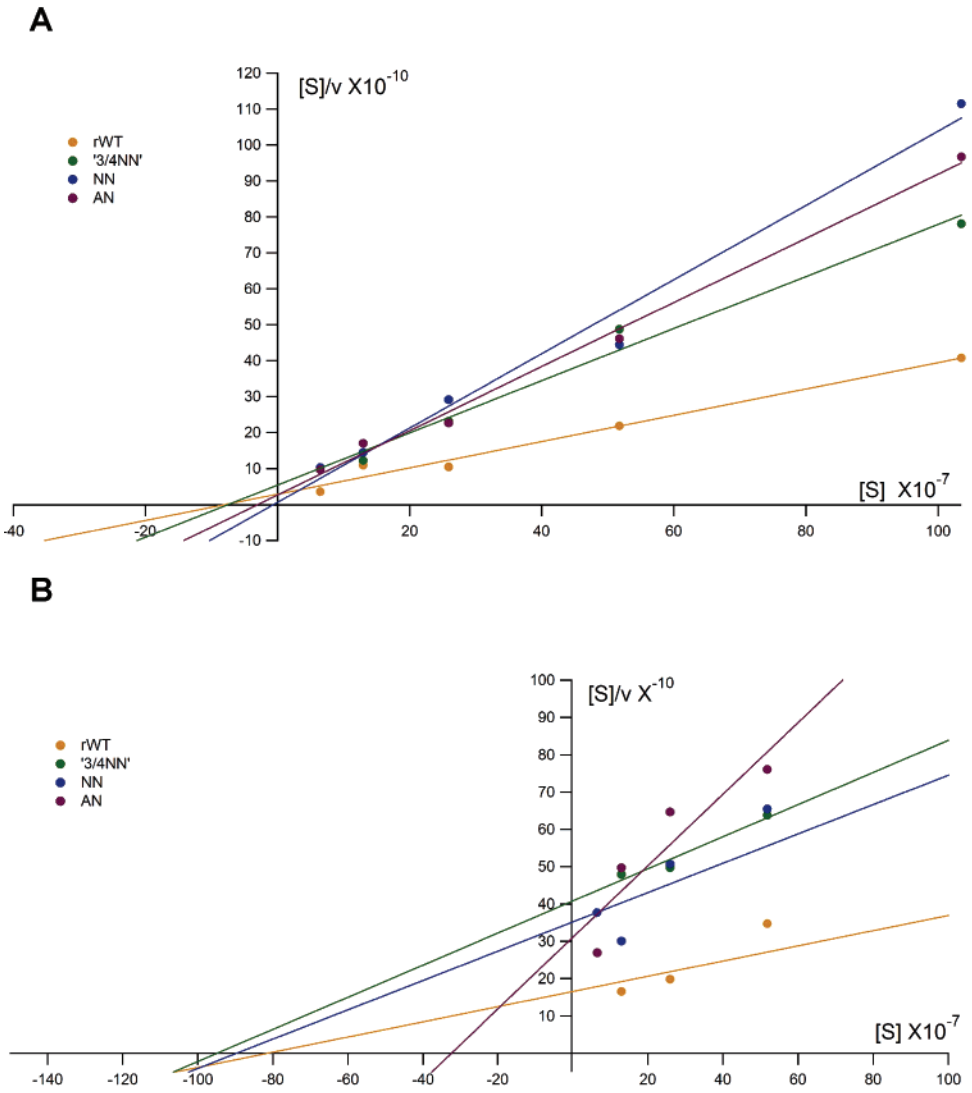

FIGURE 3: Kinetic analysis of LCAT catalyzed cholesterol esterification of POPC rHDL containing wild-type and mutant apoA-I. (A) shows the Hanes−Woolf plot for 96 Å POPC rHDL containing WT (brown), $^3/_4$ NN (green), NN (blue), and AN apoA-I (purple). (B) shows the Hanes−Woolf plot for 80 Å POPC rHDL with colored symbols defined as in panel A. Hanes−Woolf plots were used to determine the K_m, V_{max}, and catalytic efficiency (V_{max}/K_m) (Table 2) describing the LCAT reaction, where the *x*-axis is the substrate cholesterol [*S*] concentration expressed in μM and the *y*-axis is [*S*/*V*] or the substrate concentration divided by the rate of cholesterol ester formation (*V*) expressed as nanomoles of cholesterol ester formed per hour per milliliter of LCAT. All rHDL were prepared and purified as described in Figure 2. All values represent the mean ± SD of at least two separate experiments done in triplicate.

creased negative charge imparted to the rHDL by the apoA-I helix 6 AN mutation. Thus, rHDL were generated with an initial molar ratio of 76:4:5:1, POPC/POPS/cholesterol/apoA-I (POPC/POPS rHDL). The addition of 4 mol of POPS per 1 WT apoA-I molecule was chosen in order to add 8 negative charges per rHDL particle, mimicking the charge added to particles by 2 AN apoA-I molecules. In addition to these rHDL, pure POPC rHDL were also prepared using WT and AN apoA-I at initial molar ratios of 80:5:1 POPC/cholesterol/apoA-I for the generation of 96 Å particles.

Table 4 shows the final molar compositions for each of the purified rHDL. These results suggest that POPC WT, POPC AN, and POPC/POPS WT apoA-I rHDL particles were all similar in composition. Interestingly, the sizes of the rHDL were also very similar as determined by nondenaturing gradient gel electrophoresis, shown in Figure 5. These results suggest that the inclusion of POPS into the rHDL had little effect on the overall number of phospholipids molecules incorporated into the particles.

Although the inclusion of a negatively charged phospholipid did not alter the size or composition of the rHDL, the overall net particle charge was affected, as shown by agarose gel electrophoresis in Figure 6. When rHDL were separated based on particle charge, POPC/POPS WT apoA-I rHDL migrated with a similar surface potential as POPC AN apoA-I rHDL. Figure 6 shows the migration of POPC WT apoA-I (lane 1), POPC AN apoA-I rHDL (lane 2), and POPC/POPS WT apoA-I rHDL (lane 3), with a calculated surface potential corresponding to −8.2, −11.3, and −12.3 mV, respectively. Overall, these results suggest that the net rHDL particle charge in POPC AN apoA-I rHDL was similar to that contributed by the addition of the negatively charged POPS to the POPC WT apoA-I rHDL (*56*).

We next measured the LCAT activation properties for the POPC and POPC/POPS rHDL shown in Table 5. The kinetic constants, derived from Hanes−Woolf plots, suggest that POPC/POPS WT apoA-I rHDL activates LCAT in a manner

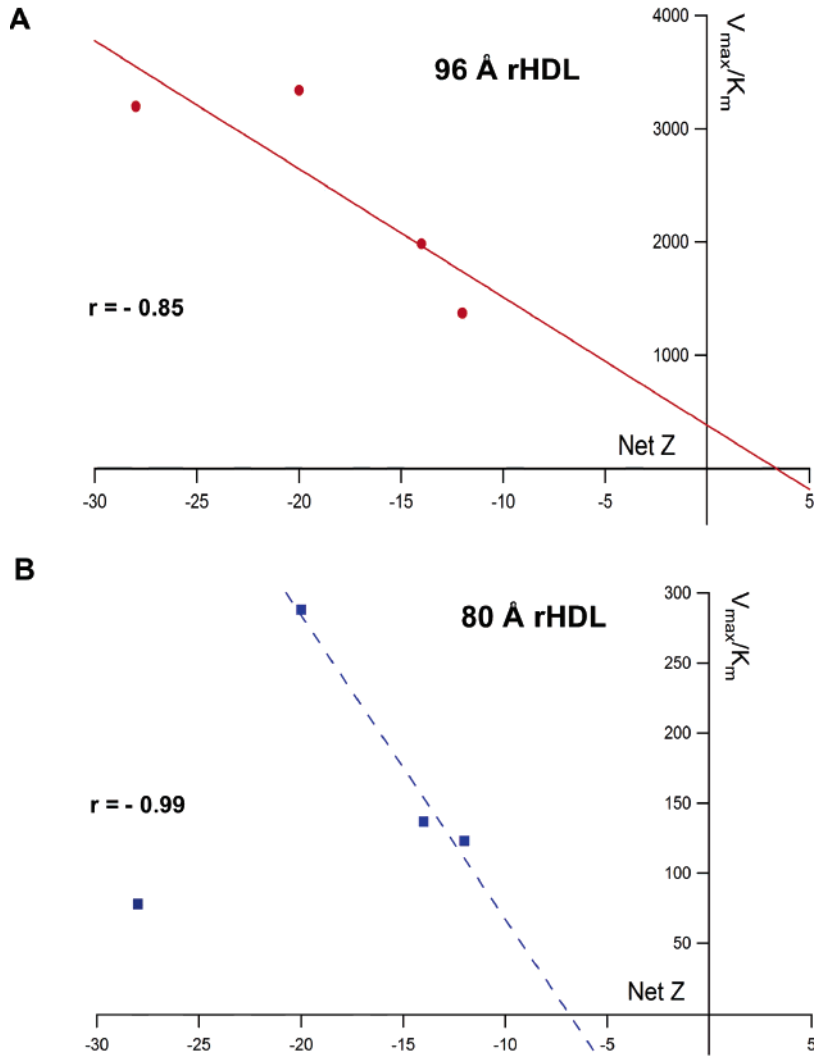

FIGURE 4: Relationship between LCAT catalytic efficiency and the net apoA-I rHDL charge. Theoretical net charge (net *Z*) of two apoA-I molecules on a single rHDL were tabulated (Table 2) and plotted against the catalytic efficiency (V_{max}/K_m) of the LCAT catalyzed cholesterol esterification reaction (Table 2). (A) Shows the relationship for 96 Å rHDL containing WT or mutant apoA-I. (B) Shows the relationship for the 80 Å rHDL containing WT or mutant apoA-I. The correlation coefficient is calculated for panel A using all four points, while for panel B, it was calculated using only three points, excluding AN apoA-I rHDL. ApoA-I net *Z* was calculated by tabulating the net charge of individual amino acids at pH = 7.4.

Table 3: ApoA-I Helix 6 Hydrophobicity, Hydrophobic Moment, and Surface Activity[a]

identity of ApoA-I helix 6 mutation[b]	helix 6 hydrophobicity[c] (kcal/mol)	helix 6 hydrophobic moment[d] (kcal/mol)	exclusion pressure (mN/m)
WT	−0.285	0.383	27 ± 0.4[e]
3/4 NN	−0.279	0.373	ND
NN	−0.284	0.373	28 ± 0.7[e]
AN	−0.513	0.468	19 ± 0.8[f]

[a] The hydrophobicity and hydrophobic moments were calculated for apoA-I helix 6 for both WT or mutant forms of apoA-I. Exclusion pressure was experimentally determined as described in Experimental Procedures and represent the mean ± SD. [b] WT apoA-I = wild-type apoA-I; 3/4 NN or 3/4 no negative apoA-I = E146Q, D150N, D157N apoA-I; NN apo A-I or no negative apoA-I = E146Q, E147Q, D150N, D157N apoA-I; AN apoA-I or all negative apoA-I = A154D, A158D, T161D, A164D apoA-I. [c] Calculated from a consensus scale described by Eisenberg et al. (53). [d] The helical hydrophobic moment was calculated as described (54). [e,f] Values with different letters were found to be statistically different at $p < 0.05$. ND = not determined.

Table 4: Recombinant HDL Compositions and Particle Size[a]

recombinant HDL discoidal complexes[b]	final POPC/ apo A-I molar ratio	final POPS/ apo A-I molar ratio	final cholesterol/ apo A-I molar ratio	particle diameter Å
POPC WT apoA-I[c]	69 ± 4		4.6 ± 0.6	96 ± 3
POPC AN apoA-I[c]	70 ± 1		4.5 ± 0.3	94 ± 3
POPC/POPS WT apoA-I[d]	64 ± 3	5 ± 1	5.0 ± 0.6	95 ± 2

[a] Final molar ratios on all rHDL were carried out after purification as described under Experimental Procedures. Each of the rHDL was found to contain two molecules of apoprotein per particle, as determined by cross-linking with dithio-bis(succinimidyl-propionate) described in Experimental Procedures. All values represent the mean ± SD. [b] Wild-type apoA-I = WT apoA-I; AN apoA-I or all negative apoA-I = A154D, A158D, T161D, A164D apoA-I. [c] The starting molar ratio for WT and AN rHDL was 80:5:1 POPC/cholesterol/WT or AN apoA-I. [d] The starting molar ratio for POPC/POPS WT apoA-I rHDL was 76:4:5:1 POPC/POPS/cholesterol/WT apoA-I.

more similar to POPC WT apoA-I, while POPC AN apoA-I rHDL showed a 2-fold reduction in the apparent LCAT reaction velocity (Table 5) when compared to POPC WT or POPC/POPS WT apoA-I rHDL. These results strongly suggest that the interaction of LCAT with POPC AN apoA-I

Table 5: Reaction Kinetics of Recombinant POPC/POPS rHDL Particles with LCAT[a]

recombinant HDL discoidal complexes[b,c]	rHDL surface charge[d] (mV)	apparent K_m (μM)	apparent V_{max} (nmol/(h mL))	apparent V_{max}/K_m (nmol/(h mL μM))	α-helicity[e] (%)
POPC WT apoA-I	−8.2	1.0 ± 0.1^{f}	3087 ± 59^{f}	3087 ± 414^{f}	$72 \pm 5^{f,h}$
POPC AN apoA-I	−11.3	0.6 ± 0.2^{g}	1777 ± 103^{g}	2906 ± 958^{f}	70 ± 3^{f}
POPC/POPS WT apoA-I	−12.3	$0.8 \pm 0.2^{f,g}$	2726 ± 305^{f}	3407 ± 897^{f}	$77 \pm 5^{g,h}$

[a] Apparent kinetic parameters were determined from Hanes−Woolf plots of reaction velocity and cholesterol concentration as described under Experimental Procedures. All values represent the mean ± SD of duplicate determinations. [b] WT apoA-I = wild-type apoA-I; AN apoA-I or all negative apoA-I = A154D, A158D, T161D, A164D apoA-I. [c] rHDL were prepared as described in Table 4. [d] rHDL surface charge was measured on 0.5% agarose gels as described in Experimental Procedures. [e] α-helicity was determined by using a Jasco J720 at 222 nm. [f−h] Values with different letters were statistically different from each other at $p < 0.05$.

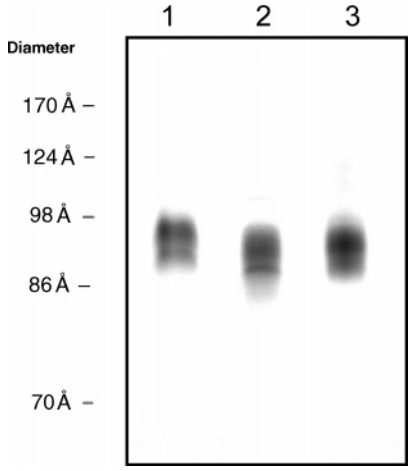

FIGURE 5: Coomassie blue stained 4−30% nondenaturing polyacrylamide gradient gel of POPC/POPS rHDL containing WT or AN apoA-I. Lane 1, POPC WT apoA-I rHDL; lane 2, POPC AN apoA-I rHDL; lane 3, POPC/POPS WT apoA-I rHDL. POPC rHDL were prepared using a starting molar ratio of 80:5:1, POPC/cholesterol/apoA-I, whereas the rHDL containing the charged phospholipid POPS was prepared in a manner similar to that described above except that the starting molar ratio was 76 mol POPC/4 mol POPS, with 5 mol cholesterol/1 mol apoA-I. All rHDL were purified by FPLC as described in Figure 2. The final molar ratios of all the rHDL as shown in Table 5 were carried out as described in Experimental Procedures. Calibrating high-molecular weight standards corresponded to a Stokes' diameter: thyroglobin, 170 Å; ferritin, 124 Å; catalase, 98 Å; lactate dehydrogenase, 86 Å; serum albumin, 74 Å.

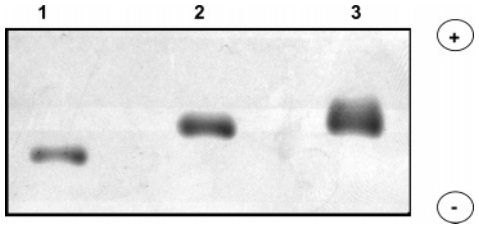

FIGURE 6: Agarose gel electrophoresis of POPC/POPS rHDL containing WT or AN apoA-I. Agarose gel electrophoresis (5%) was carried out as described in Experimental Procedures with approximately 5 μg of protein loaded in each lane. After drying, the gel was stained with Sudan Black B as described in Experimental Procedures. Lane 1 shows the migration of POPC WT apoA-I rHDL, lane 2 shows the migration of POPC AN apoA-I rHDL, and lane 3 shows the migration of POPC/POPS WT apoA-I rHDL. All POPC rHDL were prepared using a starting molar ratio of 80:5:1, POPC/cholesterol/apoA-I, whereas the rHDL containing the mixture of POPC and charged phospholipid POPS was prepared in a manner similar to that described above except that the starting molar ratio was 76 mol POPC/4 mol POPS, with 5 mol cholesterol/1 mol apoA-I. All 96 Å POPC rHDL were purified by FPLC.

rHDL is specific for apoA-I helix 6 and not the overall rHDL particle charge.

DISCUSSION

In the present study, we have shown that negatively charged amino acids within apoA-I helix 6 directly modulate the catalytic efficiency of the cholesterol esterifying enzyme LCAT. These studies also emphasize the importance of the net rHDL surface charge and its contribution to the overall conformation of lipid-bound apoA-I (*56*, *57*). We found that the removal of all four helix 6 negatively charged residues (NN apoA-I) correlated with a decrease in LCAT catalytic efficiency (Figure 3) and an increase in the apoprotein's α-helical content (Table 2). This observation may be explained by the loss of intrahelical salt bridges which would then allow helix 6 to relax or stretch from its normal conformation. In this relaxed conformation, the NN apoA-I would be expected to bind more lipid and, thus, form larger diameter rHDL (Table 1) as was observed.

The role of intrahelical salt bridges stabilizing apoA-I helix 6 seems consistent when one considers earlier studies showing that removal of helix 6 positively charged amino acids dramatically impair LCAT catalytic efficiency (*24*). Combined, these observations suggest that the role of the highly conserved negatively and positively charged amino acids within helix 6 (Figure 1) relates to the formation of intrahelical salt bridges which stabilize the 22-residue α-helical segment. It is well-known that ion pairs of the type i, $i + 3$ and i, $i + 4$ increase the conformational stability of solvent exposed α-helices (*58*); however, providing experimental evidence for the participation of specific residues in salt bridge formation is difficult without X-ray crystallography data. Despite slow progress in obtaining high-resolution crystallography data from lipid-bound complexes containing apoA-I, numerous investigations have relied upon high evolutionary conservation in the prediction of functional domains (*59*−*62*). Therefore, for apoA-I helix 6, the glutamic acids at positions 146 and 157 show >95% charge conservation across 21 different species for which apoA-I has been sequenced (Peelman, F., and Rosseneu, M., personal communication). While arginines at positions 149 and 160 show 100% charge conservation across the same 21 species, none of the other charged residues within helix 6 show this same high degree of charge conservation as seen with residues at positions 146, 149, 157, and 160. Given this high degree of evolutionary conservation, it seems reasonable to hypothesize

that glutamic acid at position 146 and arginine at position 149 may form salt bridges, as could glutamic acid 157 and arginine 160 of the *i*, *i* + 3 type. Thus, such a high degree of positional conservation suggests that these residues do play a crucial role in determining the structure and function of lipid-bound A−I.

Additionally, in support of this idea, apoA-I mutations were made in which potential helix 6 salt-bridge pairs were created and characterized (*24*). Three ion pair mutations, apoA-I E146A + R149A, apoA-I R149A + D150A, and apoA-I R153A + D150A were expressed and used in the formation of rHDL. The LCAT catalytic efficiency was measured for each of the mutant apoA-I containing rHDL, and interestingly, only apoA-I E146A + R149A reduced LCAT catalytic efficiency to the same extent as that measured when both of the highly conserved arginines (149 and 160) in helix 6 were removed (*24*). It is also highly likely that, in addition to potential intrahelical salt bridges, negatively charged helix 6 residues form intermolecular salt bridges which also function to stabilize the lipid-bound conformation of apoA-I. Computer-modeling studies (*15*, *63*) have shown that helix 6 residue E147 likely forms an ion pair with helix 4 residue K118 when folded in an extended belt conformation.

Theoretically, the addition of helix 6 negatively charged residues (AN apoA-I) could either stabilize or destabilize the conformation of the α-helical segment by favoring the formation of new or alternate salt bridges. Results from these studies indicate that on the 96 Å rHDL the effects of additional negative charge were minimal, but on 80 Å rHDL, the effects were highly significant and multifold (Figure 4). First, it has been shown that the surface charge density of WT apoA-I containing rHDL becomes more negative as the particle size decreases (*56*) presumably caused by changes in apoA-I conformation occurring as the apoprotein adapts to a smaller diameter phospholipid disc. Thus, the combination of surface constraint and additional negative charge is associated with a dramatic decrease in α-helical content, decreased surface activity (Table 3), and greatly impaired LCAT activation properties. Combined, these results suggest that the repulsion between numerous negatively charged helix 6 side chains does not allow helix 6 to make sufficient contact to form stable helix 6−LCAT interactions.

In summary, the studies described in this report delineate the role of highly conserved negatively charged residues in apoA-I helix 6 as they pertain to rHDL structure and function. The number and placement of negatively and positively charged residues within helix 6 has important implications in the stability, surface activity, and LCAT activation properties of apoA-I. The basis for this stabilization is likely related to the formation of intra- and interhelical salt bridges which likely play a critical role in the direct binding of apo A-I with LCAT.

ACKNOWLEDGMENT

The authors wish to thank Drs. Roy Hantgan and Michael Phillips for their thoughtful comments regarding LCAT kinetics, catalytic efficiency, and phospholipid charge. We also thank Dr. John Parks for providing the purified human His-LCAT.

REFERENCES

1. Boden, W. E. (2000) High-density lipoprotein cholesterol as an independent risk factor in cardiovascular disease: assessing the data from Framingham to the Veterans Affairs high-density lipoprotein intervention trial, *Am. J. Cardiol. 86*, 19L−22L.
2. Fielding, C. J., and Fielding, P. E. (1995) Molecular physiology of reverse cholesterol transport, *J. Lipid Res. 36*, 211−228.
3. Yancey, P. G., Bortnick, A. E., Kellner-Weibel, G., de la Llera-Moya, M., Phillips, M. C., and Rothblat, G. H. (2003) Importance of different pathways of cellular cholesterol efflux, *Arterioscler., Thromb., Vasc. Biol. 23*, 712−9, (Epub Jan 23, 2003).
4. Tall, A. R. (2003) ATVB In Focus: Role of ABCA1 in cellular cholesterol efflux and reverse cholesterol transport, *Arterioscler Thromb Vasc Biol. 23*, 710−711.
5. Trigatti, B., Rigotti, A., and Krieger, M. (2000) The role of the high-density lipoprotein receptor SR-BI in cholesterol metabolism, *Curr. Opin. Lipidol. 11*, 123−131.
6. Fogelman, A. M. (2004) When good cholesterol goes bad, *Nat. Med. 10*, 902−903.
7. Marcel, Y. L., and Kiss, R. S. (2003) Structure−function relationships of apolipoprotein A-I: a flexible protein with dynamic lipid associations, *Curr. Opin. Lipidol. 14*, 151−157.
8. Borhani, D. W., Rogers, D. P., Engler, J. A., and Brouillette, C. G. (1997) Crystal structure of truncated human apolipoprotein A-I suggests a lipid-bound conformation, *Proc. Natl. Acad. Sci. U.S.A. 94*, 12291−12296.
9. Li, H. H., Lyles, D. S., Thomas, M. J., Pan, W., and Sorci-Thomas, M. G. (2000) Structural determination of lipid-bound ApoA-I using fluorescence resonance energy transfer, *J. Biol. Chem. 275*, 37048−37054.
10. Klon, A. E., Jones, M. K., Segrest, J. P., and Harvey, S. C. (2000) Molecular belt models for the apoliporotein A-I Paris and Milano mutations, *Biophys. J. 79*, 1679−1685.
11. Panagotopulos, S. E., Horace, E. M., Maiorano, J. N., and Davidson, W. S. (2001) Apolipoprotein A-I adopts a belt-like orientation in reconstituted high density lipoproteins, *J. Biol. Chem. 276*, 42965−42970.
12. Maiorano, J. N., and Davidson, W. S. (2000) The orientation of helix 4 in apolipoprotein A-I-containing reconstituted high density lipoproteins, *J. Biol. Chem. 275*, 17374−17380.
13. Koppaka, V., Silvestro, L., Engler, J. A., Brouillette, C. G., and Axelsen, P. H. (1999) The structure of human lipoprotein A-I−Evidence for the "belt" model, *J. Biol. Chem. 274*, 14541−14544.
14. Tricerri, M. A., Behling Agree, A. K., Sanchez, S. A., Bronski, J., and Jonas, A. (2001) Arrangement of apolipoprotein A-I in reconstituted high-density lipoprotein disks: an alternative model based on fluorescence resonance energy transfer experiments, *Biochemisty 40*, 5065−5074.
15. Segrest, J. P., Jones, M. K., Klon, A. E., Sheldahl, C. J., Hellinger, M., De Loof, H., and Harvey, S. C. (1999) A detailed molecular belt model for apolipoprotein A-I in discoidal high density lipoprotein, *J. Biol. Chem. 274*, 31755−31758.
16. Li, H.-h., Lyles, D. S., Pan, W., Alexander, E., Thomas, M. J., and Sorci-Thomas, M. G. (2002) Apo A-I structure on discs and spheres: variable helix registry and conformational states, *J. Biol. Chem. 42*, 39093−39101.
17. Narayanaswami, V., Maiorano, J. N., Dhanasekaran, P., Ryan, R. O., Phillips, M. C., Lund-Katz, S., and Davidson, W. S. (2004) Helix orientation of the functional domains in apolipoprotein E in discoidal high density lipoprotein particles, *J. Biol. Chem. 279*, 14273−14279.
18. Garda, H. A., Arrese, E. L., and Soulages, J. L. (2002) Structure of apolipophorin-III in discoidal lipoproteins−Interhelical distances in the lipid-bound state and conformational change upon binding to lipid, *J. Biol. Chem. 277*, 19773−19782.
19. Sahoo, D., Weers, P. M., Ryan, R. O., and Narayanaswami, V. (2002) Lipid-triggered conformational switch of apolipophorin III helix bundle to an extended helix organization, *J. Mol. Biol. 321*, 201−214.
20. Klon, A. E., Segrest, J. P., and Harvey, S. C. (2002) Molecular dynamics simulations on discoidal HDL particles suggest a mechanism for rotation in the apo A-I belt model, *J. Mol. Biol. 324*, 703−721.
21. Klon, A. E., Segrest, J. P., and Harvey, S. C. (2002) Comparative models for human apolipoprotein A-I bound to lipid in discoidal high-density lipoprotein particles, *Biochemistry 41*, 10895−10905.
22. Segrest, J. P., Jones, M. K., De Loof, H., Brouillette, C. G., Venkatachalapathi, Y. V., and Anantharamaiah, G. M. (1992) The

amphipathic helix in the exchangeable apolipoproteins: a review of secondary structure and function, *J. Lipid Res. 33*, 141−166.
23. Segrest, J. P., De Loof, H., Dohlman, J. G., Brouillette, C. G., and Anantharamaiah, G. M. (1990) Amphipathic helix motif: classes and properties, *Proteins 8*, 103−117.
24. Roosbeek, S., Vanloo, B., Duverger, N., Caster, H., Breyne, J., De Beun, I., Patel, H., Vandekerckhove, J., Choulders, C., Rosseneu, M., and Peelman, F. (2001) Three arginine residues in apolipoprotein A-I are critical for activation of lecithin:cholesterol acyltransferase, *J. Lipid Res. 42*, 31−40.
25. Sparks, D. L., Anantharamaiah, G. M., Segrest, J. P., and Phillips, M. C. (1995) Effect of the cholesterol content of reconstituted LpA-I on lecithin:cholesterol acyltransferase activity, *J. Biol. Chem. 270*, 5151−5157.
26. Segrest, J. P., Li, L., Anantharamaiah, G. M., Harvey, S. C., Liadaki, K. N., and Zannis, V. (2000) Structure and function of apolipoprotein A-I and high-density lipoprotein, *Curr. Opin. Lipidol. 11*, 105−115.
27. Neves Petersen, M. T., Fojan, P., and Petersen, S. B. (2001) How do lipases and esterases work: the electrostatic contribution, *J. Biotechnol. 85*, 115−147.
28. Peters, G. H., and Bywater, R. P. (2001) Influence of a lipid interface on protein dynamics in a fungal lipase, *Biophys. J. 81*, 3052−3065.
29. Desrumaux, C., Athias, A., Masson, D., Gambert, P., Lallemant, C., and Lagrost, L. (1998) Influence of the electrostatic charge of lipoprotein particles on the activity of the human plasma phospholipid transfer protein, *J. Lipid Res. 39*, 131−142.
30. Nishida, H. I., Arai, H., and Nishida, T. (1993) Cholesterol ester transfer mediated by lipid transfer protein as influenced by changes in the charge characteristics of plasma lipoproteins, *J. Biol. Chem. 268*, 16352−16360.
31. Li, H. H., Thomas, M. J., Pan, W., Alexander, E., Samuel, M., and Sorci-Thomas, M. G. (2001) Preparation and incorporation of probe-labeled apoA-I for fluorescence resonance energy transfer studies of rHDL, *J. Lipid Res. 42*, 2084−2091.
32. Sorci-Thomas, M. G., Parks, J. S., Kearns, M. W., Pate, G. N., Zhang, C., and Thomas, M. J. (1996) High level secretion of wild-type and mutant forms of human proapoA-I using baculovirus-mediated Sf-9 cell expression, *J. Lipid Res. 37*, 673−683.
33. Sorci-Thomas, M. G., Curtiss, L., Parks, J. S., Thomas, M. J., Kearns, M. W., and Landrum, M. (1998) The hydrophobic face orientation of apolipoprotein A-I amphipathic helix domain 143−164 regulates lecithin: cholesterol acyltransferase activation, *J. Biol. Chem. 273*, 11776−11782.
34. Reschly, E. J., Sorci-Thomas, M. G., Davidson, W. S., Meredith, S. C., Reardon, C. A., and Getz, G. S. (2002) Apolipoprotein A-I alpha-helices 7 and 8 modulate high density lipoprotein subclass distribution, *J. Biol. Chem. 277*, 9645−9654.
35. Parks, J. S., and Gebre, A. K. (1991) Studies on the effect of dietary fish oil on the physical and chemical properties of low density lipoproteins in cynomolgus monkeys, *J. Lipid Res. 32*, 305−315.
36. Mingarro, I., Elofsson, A., and Von Heijne, G. (1997) Helix-helix packing in a membrane-like environment, *J. Mol. Biol. 272*, 633−641.
37. Sparks, D. L., and Phillips, M. C. (1992) Quantitative measurement of lipoprotein surface charge by agarose gel electrophoresis, *J. Lipid Res. 33*, 123−130.
38. Chisholm, J. W., Gebre, A. K., and Parks, J. S. (1999) Characterization of C-terminal histidine-tagged human recombinant lecithin:cholesterol acyltransferase, *J. Lipid Res. 40*, 1512−1519.
39. Weinberg, R. B., Cook, V. R., Jones, J. B., Kussie, P., and Tall, A. R. (1994) Interfacial properties of recombinant human cholesterol ester transfer protein, *J. Biol. Chem. 269*, 29588−29591.
40. Weinberg, R. B., Ibdah, J. A., and Phillips, M. C. (1992) Adsorption of apolipoprotein A-IV to phospholipid monolayers spread at the air/water interface. A model for its labile binding to high density lipoproteins, *J. Biol. Chem. 267*, 8977−8983.
41. Minnich, A., Collet, X., Roghani, A., Cladaras, C., Hamilton, R. L., Fielding, C. J., and Zannis, V. I. (1992) Site-directed mutagenesis and structure−function analysis of the human apolipoprotein A-I. Relation between lecithin-cholesterol acyltransferase activation and lipid binding, *J. Biol. Chem. 267*, 16553−16560.
42. Sorci-Thomas, M., Kearns, M. W., and Lee, J. P. (1993) Apolipoprotein A-I domains involved in lecithin-cholesterol acyltransferase activation. Structure: function relationships, *J. Biol. Chem. 268*, 21403−21409.
43. Sorci-Thomas, M. G., Thomas, M., Curtiss, L., and Landrum, M. (2000) Single repeat deletion in apoA-I blocks cholesterol esterification and results in rapid catabolism of Δ6 and wild-type apoA-I in transgenic mice, *J. Biol. Chem. 275*, 12156−12163.
44. Sorci-Thomas, M. G., and Thomas, M. J. (2002) The effects of altered apolipoprotein A-I structure on plasima HDL concentration, *Trends Cardiovasc. Med. 12*, 121−128.
45. Asztalos, B. F., Sloop, C. H., Wong, L., and Roheim, P. S. (1993) Two-dimensional electrophoresis of plasma lipoproteins: recognition of new apo A-I-containing subpopulations, *Biochim. Biophys. Acta 1169*, 291−300.
46. Asztalos, B. F., Sloop, C. H., Wong, L., and Roheim, P. S. (1993) Comparison of apo A-I-containing subpopulations of dog plasma and prenodal peripheral lymph: evidence for alteration in subpopulations in the interstitial space, *Biochim. Biophys. Acta 1169*, 301−304.
47. Arnulphi, C., Jin, L., Tricerri, M. A., and Jonas, A. (2004) Enthalpy-driven apolipoprotein A-I and lipid bilayer interaction indicating protein penetration upon lipid binding, *Biochemistry 43*, 12258−12264.
48. Davidson, W. S., Hazlett, T., Mantulin, W. W., and Jonas, A. (1996) The role of apolipoprotein AI domains in lipid binding, *Proc. Natl. Acad. Sci. U.S.A. 93*, 13605−13610.
49. Gorshkova, I. N., Liu, T., Zannis, V. I., and Atkinson, D. (2002) Lipid-free structure and stability of apolipoprotein A-I: probing the central region by mutation, *Biochemistry 41*, 10529−10539.
50. Calabresi, L., Franceschini, G., Burkybile, A., and Jonas, A. (1997) Activation of lecithin cholesterol acyltransferase by a disulfide-linked apolipoprotein A-I dimer, *Biochem. Biophys. Res. Commun. 232*, 345−349.
51. Jonas, A., Kezdy, K. E., and Wald, J. H. (1989) Defined apolipoprotein A-I conformations in reconstituted high density lipoprotein discs, *J. Biol. Chem. 264*, 4818−4824.
52. Jonas, A., Wald, J. H., Toohill, K. L., Krul, E. S., and Kezdy, K. E. (1990) Apolipoprotein A-I structure and lipid properties in homogeneous, reconstituted spherical and discoidal high density lipoproteins, *J. Biol. Chem. 265*, 22123−22129.
53. Eisenberg, D. (1984) Three-dimensional structure of membrane and surface proteins, *Annu. Rev. Biochem. 53*, 595−623.
54. Eisenberg, D., Weiss, R. M., and Terwilliger, T. C. (1982) The helical hydrophobic moment: a measure of the amphiphilicity of a helix, *Nature 299*, 371−374.
55. Krebs, K. E., Ibdah, J. A., and Phillips, M. C. (1988) A comparison of the surface activityes of human apolipoproteins A-I and A-II at the air/water interface, *Biochim. Biophys. Acta 959*, 229−237.
56. Sparks, D. L., Lund-Katz, S., and Phillips, M. C. (1992) The charge and structural stability of apolipoprotein A-I in discoidal and spherical recombinant high density lipoprotein particles, *J. Biol. Chem. 267*, 25839−25847.
57. Sparks, D. L., Frank, P. G., and Neville, T. A. M. (1998) Effect of the surface lipid composition of reconstituted LPA-I on apolipoprotein A-I structure and lecithin: cholesterol acyltransferase activity, *Biochim. Biophys. Acta 1390*, 160−172.
58. Fasman, G. D. (1989) in *Prediction of Protein Structure and the Principles of Protein Conformation* (Fasman, G. D., Ed.) pp 193−301, Plenum Press, New York and London.
59. Collet, X., Marcel, Y. L., Tremblay, N., Lazure, C., Milne, R. W., Perret, B., and Weech, P. K. (1997) Evolution of mammalian apolipoprotein A-I and conservation of antigenicity: correlation with primary and secondary structure, *J. Lipid Res. 38*, 634−644.
60. O'hUigin, C., Chan, L., and Li, W.-H. (1990) Cloning and sequencing of bovine apolipoprotein A-I cDNA and molecular evolution of apolipoproteins A-I and B-100, *Mol. Biol. Evol. 7*, 327−339.
61. Luo, C.-C., Li, W.-H., Moore, M., and Chan, L. (1986) Structure and evolution of the apolipoprotein multigene family, *J. Mol. Biol. 187*, 325−340.
62. von Eckardstein, A., Funke, H., Walter, M., Altland, K., Benninghove, A., and Assmann, G. (1990) Structural analysis of human apolipoprotein A-I variants. Amino acid substitutions are nonrandomly distributed throughout the apolipoprotein A-I primary structure, *J. Biol. Chem. 265*, 8610−8617.
63. Li, L., Chen, J., Mishra, V. K., Kurtz, J. A., Cao, D., Klon, A. E., Harvey, S. C., Anantharamaiah, G. M., and Segrest, J. P. (2004) Double belt structure of discoidal high density lipoproteins: molecular basis for size heterogeneity, *J. Mol. Biol. 343*, 1293−1311.

BI047412V